Characterization of supercontinuum generation along a silica tapered optical fiber using a confocal micro-spectrometer

Yosri Haddad, Thibaut Sylvestre, Jean-Charles Beugnot, Samuel Margueron, Gil Fanjoux

Characterization of supercontinuum generation along a silica tapered optical fiber using a confocal micro-spectrometer

Yosri Haddad[1], Thibaut Sylvestre[1], Jean-Charles Beugnot[1], Samuel Margueron[1], and Gil Fanjoux[1]

[1]Institut FEMTO-ST, UMR 6174 CNRS / Université Bourgogne Franche-Comté, 25030 Besançon, France

ABSTRACT

We have characterized the supercontinuum generation along a tapered silica optical fiber using a highly-sensitive distributed measurement technique. Based on a confocal Raman micro-spectrometer, this method involves far-field point-by-point Rayleigh scattering analysis along the waveguide, providing micrometer spatial resolution and high spectral resolution. This non-destructive and non-invasive technique enables the observation of each step of supercontinuum generation along the fiber taper.

1. INTRODUCTION

Supercontinuum (SC) generation in optical nonlinear waveguides has been largely studied and underlying linear and nonlinear physical processes are now well understood.[1–3] Therefore, SC spectra measured with an optical spectrum analyzer (OSA) at the output of a nonlinear waveguide are generally well-modeled by numerical simulations based on the generalized nonlinear Schrödinger equation (GNLSE).[2] However, even if the guided light can be perfectly characterized at the waveguide output spectrally, in power, and in polarization, its longitudinal evolution all along the waveguide is difficult to access. Therefore, some parameters of the numerical model are fitted only with the waveguide output spectra. The knowledge of the longitudinal evolution of the field along the waveguide represents a higher level of test for numerical models and for the determination of some numerical parameters. Although some techniques already exist to measure broad spectra with nanometric spatial resolution along sub-millimetric nonlinear waveguides with a SNOM,[4] or along optical fibers with a metric resolution with a modified OTDR,[5] no non-destructive and non-invasive technique exists for centimetric nonlinear waveguides. For that purpose, we recently developed a new experimental technique allowing longitudinal spectral measurements of light propagating in an optical waveguide with a micrometric spatial resolution and sub-nanometric spectral resolution.[6] Note that our system has the same performance as the state-of-the-art OBR system,[7] or the imaging system of Rayleigh scattered light with an EMCCD camera,[8] with however the great added benefit of spectral analysis combined with the spatial dimension.

We then apply this technique in this work to analyze the generation of SC along a tapered fiber already studied in a classic way.[9,10] More precisely, the objective of this work concerns the distributed spectral measurements of the field intensity guided along a tapered fiber in the SC generation regime in order to confront measured spectra with numerical simulations and demonstrate the high performance of our system. These distributed spectra observations especially allow the accurate analysis of the contributions of different parts making up the tapered fiber, i.e., the homogeneous diameter part called thereafter the optical nanofiber (ONF), and the transitions between the standard fiber and the ONF. We observe in particular the generation of a large Raman cascading effect in the anti-Stokes side in the first transition between the input standard fiber and the ONF, followed by the generation of a dispersive wave localized in the ONF which contributes to SC generation. All these experimental observations are successfully compared with numerical simulations. All these measurements prove the importance of longitudinal measures along an optical waveguide in a nonlinear regime to refine understanding and then numerical models.

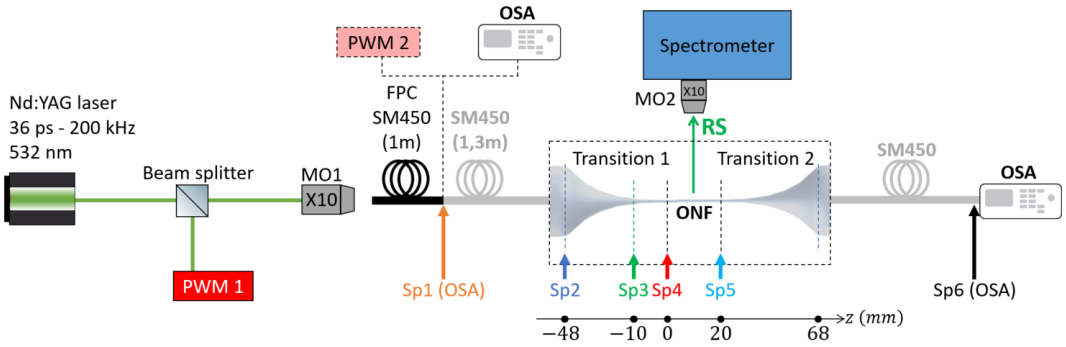

Figure 1. Experimental setup. PWM, power meter; FPC, fiber patchcord; ONF, optical nanofiber; OSA, optical spectrum analyzer; MO1 and MO2, microscope objectives; Spi, spectrum number i; RS, Rayleigh scattering signal collected by the spectrometer.

2. EXPERIMENTAL SETUP

The experimental setup is drawn in Figure 1. The analysis system has already been described in Ref.[6] To resume, it consists of a confocal Raman micro-spectrometer (Monovista, S-&-I GmbH) used to detect the Rayleigh scattering (RS) fields of all the spectral components guided in the waveguide in the direction perpendicular to the waveguide, except the intense pump field filtered by three Notch filters. The system is equipped with a high-precision motorized stage for the 3D displacements of the waveguide under study, all with a step size and replicability better than 100 nm. This system allows the generation of an accurate recordable 3D spatial trajectory point-by-point all along the waveguide. Therefore, after having recorded the waveguide trajectory, the system allows us to measure a $1D$ RS trace along the waveguide. The RS of the guided light in the optical waveguide medium exiting to the outside of the waveguide is collected at the right angle to the propagation direction (Fig. 1) with a $\times 10$ microscope objective and recorded through the spectrometer. The monochromator is equipped with a 300 lines/mm diffraction grating for that work, and a back-illuminated cooled CCD detector (-85C) leading to a low detection threshold and a high signal-to-noise ratio (SNR). The entrance slit width of the confocal spectrometer has been fixed to 1 mm for maximal signal intensity. At best, our system has a spatial resolution of 5 μm and a spectral resolution of 0.2 nm.

The optical nanofiber (ONF) is manufactured by tapering a standard single-mode fiber in the visible range (SM450) using the heat-brush technique.[11–14] The optical losses measured just after manufacturing remain below about 0.2 dB at 532 nm of wavelength, ensuring that the transitions are adiabatic for the fundamental mode at the pump laser wavelength. Just after manufacturing, ONF is placed inside a closed transparent plexiglass box in order to protect it from external air vibrations and to reduce any kind of contamination (dust and humidity principally).[15] The ONF presents a diameter equal to 690 nm with 2% of precision (SEM measurements[6]) and homogeneous over 2 cm length, linked to the standard fiber on either side by two 48 mm long transitions with a specific variation of the diameter measured by SEM.[6] Note that a 0.5 m-long patch cord (SM450) is spliced to the stretched fiber input, leading to a standard fiber length of approximately 1.3 m before the transition 1 (Fig. 1). The whole system called thereafter *fiber system* is then composed of the ONF, the two transitions before and after the ONF, and the two standard fiber SM450 parts before and after the transitions (from Sp1 to Sp6, see Fig. 1).

The fiber system is pumped with a pulsed (36 ps, repetition rate of 200 MHz) and frequency-doubled (pump wavelength $\lambda_p = 532$ nm) Nd:YAG laser. During the measurements, we continuously monitor the pump laser power in order to control the stability of the pump source (PWM1 in Fig. 1), and the output spectra with an OSA in order to control the stability of the SC. The laser beam is first injected in a 1 m-long SM450 patch cord connected to the fiber system with a mating sleeve. This patch cord allows us to measure the input power (PWM2 in Fig. 1) and the input Raman spectrum of the fiber system.

The spectral measurements are realized with an OSA at the output of the SM450 patch cord (Sp1 in Fig. 1), and continuously when measuring RS spectra at the output of the fiber system (Sp6 in Fig. 1). As the stability of the SC is limited in time (certainly due to thermal effects), we have, therefore, decided to measure RS spectra

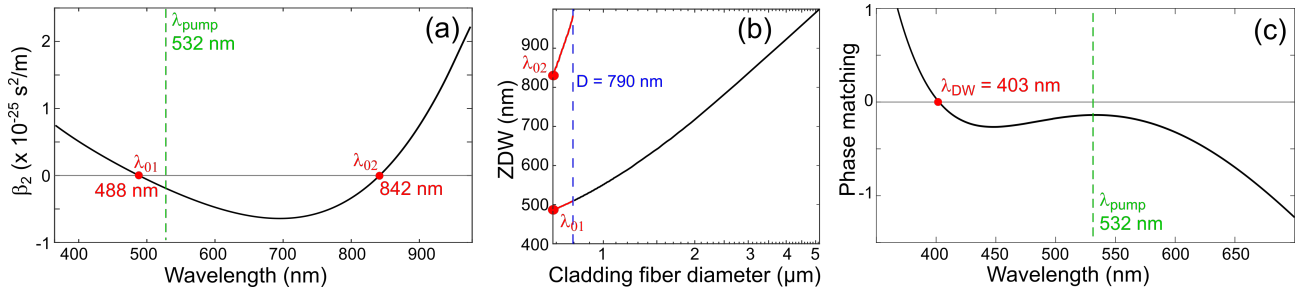

Figure 2. (a) Group velocity dispersion parameter β_2 with wavelength for the ONF diameter of 690 nm. (b) Zero dispersion wavelength (ZDW) evolution with cladding fiber diameter. Ranges of cladding fiber diameter characterized by one ZDW (black curve) or two ZDW (red curves) with the threshold represented by the vertical dashed blue line corresponding to the diameter of 790 nm. (c) Phase matching condition for dispersive wave (DW) generation according to wavelength.

at the input of the transition 1 (Sp2 in Fig. 1), 1 cm before the input of the ONF (Sp3 in Fig. 1), the input of the ONF (Sp4 in Fig. 1), and at the output of ONF (Sp5 in Fig. 1), only. Note that Sp2 to Sp5 are composed of three associated spectra in order to cover the large spectral range. Therefore, the acquisition time for Sp3, Sp4, and Sp5 is equal to 3 min, and 10 min for Sp2 due to the low level of light scattered by the core of the standard fiber.

3. NUMERICAL SIMULATIONS

In order to compare the longitudinal measurements with numerical simulations, we modeled with the generalized nonlinear Schrödinger equation (GNLSE) the light propagation in the fiber system. The slowly varying envelope $A(z,T)$ of the total electric field of the electromagnetic wave propagating in the z direction and in the pump pulse temporal frame T verifies the GNLSE equation

$$\frac{\partial A}{\partial z} = i\sum_{n=2}^{\infty} i^n \frac{\beta_n}{n!}\frac{\partial^n A}{\partial T^n} + i\gamma(1-f_R)|A|^2 A + i\gamma f_R A\int_0^{\infty} h_R(T)\,|A|^2\,dt \tag{1}$$

with β_n the n^{th} derivative of the propagation constant β, $h_R(T)$ the delayed temporal Raman response, and f_R the contribution of the Raman effect to the Kerr effect evaluated to 0.18 for standard silica fibers. The nonlinear coefficient of the fiber γ is calculated with the relation $\gamma = 2\pi n_2/(\lambda A_{eff})$ with n_2 the nonlinear index of the silica and A_{eff} the effective area of the fundamental mode evolving along the fiber system. The propagation constants $\beta(\omega) = n_{eff}\omega/c$ (c the light velocity in vacuum) have been calculated from the fundamental mode effective indices n_{eff} for each wavelength and each fiber diameter simulated by the finite element method, taking into account the geometry of the ONF and transitions.[6]

Figure 2(a) shows the wavelength-dependent evolution of the group-velocity dispersion parameter β_2 for the ONF with the diameter $D_{ONF} = 690\ nm$. This dispersion curve presents two zero dispersion wavelengths (ZDW) $\lambda_{01} = 488\ nm$ and $\lambda_{02} = 842\ nm$, with an anomalous dispersion at the pump wavelength. It is noteworthy that the ZDW strongly evolve from the standard SM450 fiber up to the ONF (Figure 2(b)). When the cladding diameter of the fiber decreases from 125 m to 690 nm, the ZDW λ_{01} decreases from around 1300 nm to 488 nm, influencing the nonlinear dynamics in the fiber transition 1 as explained thereafter. The second ZDW λ_{02} appears from a diameter of 790 nm, leading to an anomalous dispersion between the two ZDWs (Figure 2(a)).

Due to the anomalous dispersion and the proximity of the pump wavelength to λ_{01}, solitonic fission dynamics occur leading to the generation of a SC and the amplification of a dispersive wave (DW) by a four-wave mixing process (FWM) preferentially on the short wavelength side.[16] Moreover, for effective amplification of the DW, it must be phase-matched with the solitons, in accordance with the following phase-matching equation

$$\beta(\omega) - \beta(\omega_p) - \beta(\omega - \omega_{soliton}) - \gamma_{NL}P_s = 0 \tag{2}$$

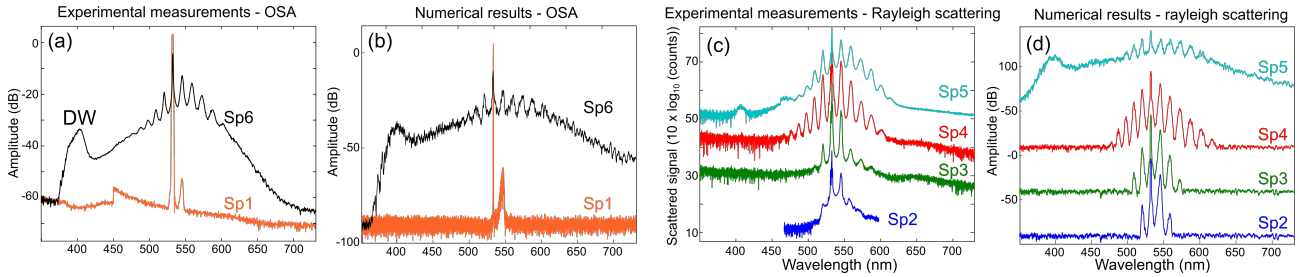

Figure 3. (a-b) Experimental spectra and (c-d) results of numerical simulations at the input (Sp1, orange curve) and at the output (Sp5, blue curve) of the fiber system, at the input of the transition 1 (Sp2, green curve), at the input of the nanofiber (Sp3, black curve), and at the end of the nanofiber (Sp4, red curve). Spectra in (b) and (d) are vertically shifted for clarity. DW, dispersive wave.

with $\beta(\omega_p)$ the propagation constant for the pump, and γ_{NL} the nonlinear coefficient. $\omega_{soliton}$ and P_s correspond to the pulsation and peak power of the fundamental soliton, respectively. $\omega_{soliton}$ was set to the pump wavelength, as no significant soliton self-frequency shift was observed in numerical simulations. Figure 2(c) represents the wavelength-dependent phase-matching. It is clear that the phase matching condition is verified for a wavelength of about 403 nm for an estimated soliton peak power of $P_s = 2000\ W$ corresponding to the mean of the highest peak powers of the ejected temporal solitons observed in the numerical simulations propagating in the ONF.

4. RESULTS AND DISCUSSIONS

Figures 3(a-d) show the spectra Sp1 to Sp6 experimentally acquired by the OSA (Fig. 3(a)) or by our system (Fig. 3(c)), and numerically simulated (Figs. 3(b) and (d)).

First, for an input peak power equal to around 340 W, the 1 m-long SM450 patchcord generates the first Raman Stokes order clearly visible in Sp1, experimental (Fig. 3(a)) and numerical (Fig. 3(d)), with the same pump peak power in order to be as close as possible to the experimental conditions.

At the input of transition 1, Sp2 in Fig. 3(c) shows that a weakly-developed Raman cascade is generated, with two Raman Stokes orders and one Raman anti-Stokes order. The numerical spectrum (Sp2 in Fig. 3(d)) shows a similar spectrum. Remember that the anti-Stokes components are generated by the four-wave mixing (FWM) process. To obtain the necessary phase matching between the Raman Stokes components, the phase mismatch due to chromatic dispersion must be balanced by the nonlinear Kerr phase, leading to the large difference in intensity between the Raman Stokes orders and the corresponding Raman anti-Stokes orders (≈ 15 dB).

One centimeter before the end of transition 1, Sp3 in Fig. 3(c) shows the development of the Raman cascade with four Raman Stokes orders and two Raman anti-Stokes orders. At this position, the diameter of the fiber is equal to about 1.53 m and the ZDW λ_{01} is positioned at about 665 nm (Fig. 2). This decrease of λ_{01}, and consequently the dispersion, allows the development of the Raman cascade. At that position, it is important to note that, to ensure that the numerical spectrum agrees with the experimental one (Sp3 in Fig. 3(d)), an attenuation of the field strength of around 2.2 dB at the transition 1 input is required. A drastic saturation and divergence of the numerical spectrum occur without these losses. The need for numerical losses can be explained by the losses of about 2.5 dB experimentally measured in the nonlinear regime, related to the observation of light rings scattered outside the fiber at the level of the transition 1, certainly due to high order leaky modes. This point is important because the distributed measurements require us to obtain numerical results in agreement with these measurements all along the waveguide and therefore need to refine our numerical model parameters.

At the end of transition 1, Sp4 clearly shows a weak development of the Raman cascade on the Stokes side compared to Sp3, but a large development on the anti-Stokes side. This is due to the sweep by the ZDW λ_{01} of the spectral range where spectral components of the Raman cascade are present. The phase mismatch due to dispersion between Stokes and anti-Stokes consequently decreases, implying the increase in the efficiency of the FWM process between Stokes and anti-Stokes components, leading to large amplification of the anti-Stokes components. The Stokes/anti-Stokes intensity difference has decreased and now averages to 6 dB for all the Stokes-anti-Stokes order couples. This specific behavior is numerically predicted (Sp4 in Fig. 3(d)). Each

Raman Stokes and anti-Stokes order pair has slightly different intensities, proving that chromatic dispersion is low. Consequently, the anti-Stokes Raman cascade is as developed as the Stokes one (five orders), which is remarkable.

After propagation in the ONF, Sp5 (Fig. 3(c)) shows the appearance of a broad peak centered at around 406 nm, attributed to the amplification of a DW, in relative agreement with the analytical prediction shown in Fig. 2(c). The anti-Stokes Raman cascade is also well developed and a SC begins to be generated. Numerically, the DW is centered at around 400 nm (Sp5 in Fig. 3(d)). The experimental-numerical agreement confirms that our numerical model is based on right dispersion parameters.

Finally, the output spectrum profile measured with the OSA (Sp6 in Fig. 3(a)) is in agreement with the numerical one (Sp6 in Fig. 3(b)). The DW maximum is centered at around 403 nm in agreement with the wavelength value at the end of the ONF (experimental Sp5).

Between the output of the ONF and the output of the fiber system (numerical Sp5 and Sp6, resp.), no drastic change is observable. This signifies that transition 2 does not significantly impact the nonlinear effects occurring in the transition. It is obvious that the increase in the effective area of the guided mode decreases definitively the pump and Raman component intensity and consequently the nonlinear effects.

5. CONCLUSION

To resume, we have experimentally studied, for the first time to our knowledge, the generation of a supercontinuum along a nanofiber with distributed spectral measurements, with a good agreement with numerical simulations. Our new experimental technique for distributed measurements of the spectral evolution of light guided in a waveguide allows one to confirm the importance of each part of the whole waveguide. In the ONF case, the SC generation needs first to have a developed Raman cascade at the input of the transition 1 (need of 2 Raman Stokes orders), in order to efficiently seed the FWM process occurring in the transition 1. This process thus generates an anti-Stokes cascade as wide as the Stokes one due to the large dispersion decrease. Consequently, all these processes allow the development of a SC with the amplification of a dispersive wave in the ONF. Furthermore, we also detect additional spectral signatures of nonlinear processes which occur only at the level of the nanofiber and not detected at the output. From a general point of view, this opens up prospects for proving the existence and efficiency of localized physical phenomena in specific nonlinear waveguides.

Funding

This project has received funding from the Agence Nationale de la Recherche (ANR) (ANR-16-CE24-0010, ANR-15-IDEX-0003, EUR EIPHI Graduate School ANR-17-EURE-0002), the Horizon Europe Framework Programme (VISUAL project 101135904) and Bourgogne Franche-Comt Region.

Disclosures

The authors declare no conflicts of interest.

REFERENCES

[1] Alfano, R. R., [*The supercontinuum laser source: the ultimate white light*], Springer Nature (2023).

[2] Dudley, J. M. and Taylor, J. R., [*Supercontinuum generation in optical fibers*], Cambridge University Press (2010).

[3] Sylvestre, T., Genier, E., Ghosh, A. N., Bowen, P., Genty, G., Troles, J., Mussot, A., Peacock, A. C., Klimczak, M., Heidt, A. M., et al., "Recent advances in supercontinuum generation in specialty optical fibers," *JOSA.B* **38**(12), F90–F103 (2021).

[4] Coillet, A., Meisterhans, M., Jager, J.-B., Petit, M., Dory, J.-B., Noé, P., Grelu, P., and Cluzel, B., "Near-field imaging of octave-spanning supercontinua generation in silicon nitride waveguides (conference presentation)," in [*Nanophotonics VII*], **10672**, 106720L, International Society for Optics and Photonics (2018).

[5] Hontinfinde, R., Coulibaly, S., Megret, P., Taki, M., and Wuilpart, M., "Nondestructive distributed measurement of supercontinuum generation along highly nonlinear optical fibers," *Optics letters* **42**(9), 1716–1719 (2017).

[6] Haddad, Y., Chrétien, J., Beugnot, J.-C., Godet, A., Phan-Huy, K., Margueron, S., and Fanjoux, G., "Microscopic imaging along tapered optical fibers by right-angle rayleigh light scattering in linear and nonlinear regime," *Optics Express* **29**(24), 39159–39172 (2021).

[7] Lai, Y.-H., Yang, K. Y., Suh, M.-G., and Vahala, K. J., "Fiber taper characterization by optical backscattering reflectometry," *Opt. Exp.* **25**(19), 22312–22327 (2017).

[8] Hoffman, J. E., Fatemi, F. K., Beadie, G., Rolston, S. L., and Orozco, L. A., "Rayleigh scattering in an optical nanofiber as a probe of higher-order mode propagation," *Optica* **2**(5), 416–423 (2015).

[9] Birks, T., Wadsworth, W., and Russell, P. S. J., "Supercontinuum generation in tapered fibers," *Optics Letters* **25**(19), 1415–1417 (2000).

[10] Foster, M., Dudley, J., Kibler, B., Cao, Q., Lee, D., Trebino, R., and Gaeta, A., "Nonlinear pulse propagation and supercontinuum generation in photonic nanowires: experiment and simulation," *Applied Physics B* **81**(2), 363–367 (2005).

[11] Tong, L., Gattass, R. R., Ashcom, J. B., He, S., Lou, J., Shen, M., Maxwell, I., and Mazur, E., "Subwavelength-diameter silica wires for low-loss optical wave guiding," *Nature* **426**(6968), 816–819 (2003).

[12] Tong, L. and Sumetsky, M., [*Subwavelength and nanometer diameter optical fibers*], Springer Science & Business Media (2011).

[13] Shan, L., Pauliat, G., Vienne, G., Tong, L., and Lebrun, S., "Stimulated raman scattering in the evanescent field of liquid immersed tapered nanofibers," *Applied Physics Letters* **102**(20), 201110 (2013).

[14] Godet, A., Ndao, A., Sylvestre, T., Pecheur, V., Lebrun, S., Pauliat, G., Beugnot, J.-C., and Huy, K. P., "Brillouin spectroscopy of optical microfibers and nanofibers," *Optica* **4**(10), 1232–1238 (2017).

[15] Bouhadida, M., Delaye, P., and Lebrun, S., "Long-term optical transmittance measurements of silica nanofibers," *Optics Communications* **500**, 127336 (2021).

[16] Mussot, A., Beaugeois, M., Bouazaoui, M., and Sylvestre, T., "Tailoring strong cw supercontinuum in photonic crystal fibers with two zero dispersion wavelengths," *Opt. Express* **15**, 11553–11563 (2007).